

Article

Scaling Law in Laser-Induced Shock Effects of NiTi Shape Memory Alloy

Xi Wang ^{1,*}, Weiguang Xia ², Xianqian Wu ³ and Chenguang Huang ³

¹ School of Mechanical, Electronic and Control Engineering, Beijing Jiaotong University, Beijing 100044, China

² The 38th Research Institute of China Electronic Technology Corporation, Hefei 230088, China; xwg0601@163.com

³ Key Laboratory for Mechanics in Fluid Solid Coupling Systems, Institute of Mechanics, Chinese Academy of Sciences, Beijing 100190, China; wuxianqian@imech.ac.cn (X.W.); huangcg@imech.ac.cn (C.H.)

* Correspondence: wangxi@bjtu.edu.cn; Tel./Fax: +86-10-5168-3195

Received: 29 January 2018; Accepted: 6 March 2018; Published: 10 March 2018

Abstract: The shock effects in laser shock processing of NiTi shape memory alloy were studied by dimensional analysis and finite element simulation. The essential dimensionless parameters controlling the residual stress distribution and plastically affected depth were found to be dimensionless pressure duration and peak pressure. By adopting the constitutive model considering the martensitic transformation and plasticity of deformation induced martensite, the influence of dimensionless parameters on the shock effects of shape memory alloy was studied numerically. The numerical results reveal the scaling law of shock effects on those dimensionless parameters quantitatively and the relationship between the plastically affected depth and peak pressure was validated with experimental results. A window of the optimal processing parameters could be obtained based on this study.

Keywords: shape memory alloy; laser shock peening; dimensionless parameters; residual stress; plastically affected depth

1. Introduction

As one of the most popular active materials, shape memory alloys (SMAs) have been increasingly used as candidate materials for biomedical devices and structural applications. Their unique properties such as shape memory and superelastic effects are derived from a thermoelastic martensitic transformation between a high-temperature, high-symmetry austenite phase and a low-temperature, low-symmetry martensite phase [1]. Besides lowering the temperature, by stressing the material in austenite phase, the martensite structures could be formed at a temperature higher than the martensite start temperature due to plastic deformation. If this martensite structure, so-called deformation induced martensite (DIM), is stable upon unloading, it could strengthen the material. Several severe plastic deformation methods have been used in NiTi alloys to induce DIM and improve its stability, such as shot peening [2], cold rolling [3], high pressure torsion [4], and equal channel angular extrusion [5]. Recently, DIM generated by laser shock peening (LSP) in NiTi alloys has been reported [6,7]. This makes LSP to have a great potential to treat SMA materials and generate localized DIM structure for practical applications.

LSP is an advanced surface enhancement technique for metals which has been widely adopted in aerospace and automobile industries to improve mechanical properties of key components [8–10]. As shown in Figure 1, during a typical LSP process, a laser pulse is focused into a high power density irradiation onto an absorption layer coated on the metallic target surface through a sheet of transparent confining layer. The heated surface is vaporized and then is transformed into plasma by ionization. The

plasma is constrained between the confining layer and the rest part of the target and continues to absorb the laser energy. The pressure generated by the plasma is transmitted to the target material through shock waves. Generally the plasma pressure can reach up to several GPa in tens of nanoseconds. Accompanied with the propagation of the shock pressure, plastic deformation occurs in a surface layer of the metallic target material and results in a certain distribution of residual stress throughout the plastically affected depth. For traditional metallic materials such as aluminum alloy, titanium alloy and stainless steel, there have been extensive experimental studies which investigated the influence of parameter such laser spot shape and its intensity on the shock effect [9]. Analytical models based on the physics of LSP process have also been developed to predict the residual stress distribution and plastically affected depth as a function of laser shock parameters [11–13]. However, the shock effects for shape memory alloys were barely studied either experimentally or analytically in the literature.

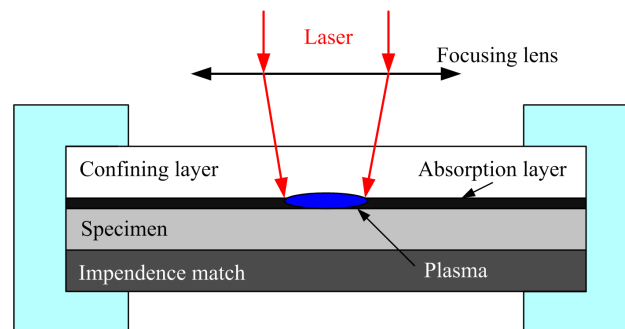


Figure 1. Schematic of laser shock peening.

It is practically useful to determine the optimized laser shock processing parameters and the corresponding peening effects for SMAs. However, it is time consuming to conduct trial experiments. Moreover, it is difficult to determine optimized parameters by theoretical analysis because LSP is a complex process influenced by multiple parameters such as laser parameters and material parameters. In this study, a scaling law for laser-shock-induced peening effects in NiTi alloys was presented with the dimensional analysis and finite element modeling. The peening effects in terms of the dimensionless variables are validated with experimental measurements of hardness-depth profile of LSP treated NiTi alloys.

2. Dimensional Analysis of LSP Process of SMAs

Based on the physics process, dimensional analysis method was used to analyze the LSP process of NiTi SMAs. The parameters controlling the effect of LSP are described as follows. For the laser induced shock, the related parameters are shock peak pressure P_m , pressure duration τ , and the radius of laser spot size R .

There are 11 parameters related with the constitutive behavior of shape memory alloy material (see Figure 2) [1]. They are austenite elastic modulus E_A , martensite elastic modulus E_M , density ρ , Poisson's ratio ν , the start stress of transformation σ_s^{AM} , the finish stress of transformation σ_f^{AM} , the start stress of reverse transformation σ_s^{MA} , the finish stress of reverse transformation σ_f^{MA} , the transformation hardening modulus E_{tr} , the yield stress of deformation induced martensite σ_y^M , and the plastic modulus E_p . The bulk compressive behavior of the target material is assumed to be described by hydroelastoplastic model, so the material parameters also include Mie-Grüneisen equation of state (EOS) coefficient γ , b_A , c_A , b_M , and c_M .

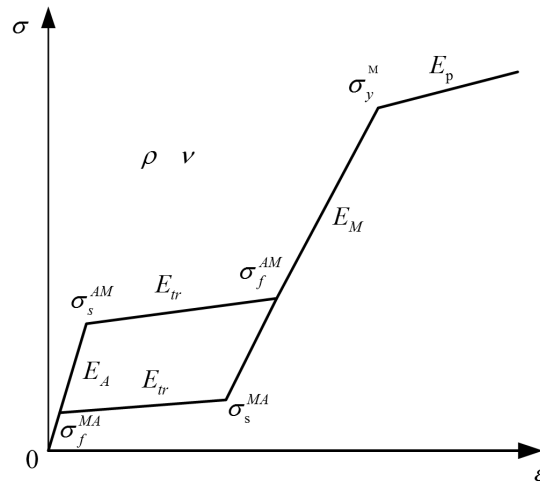


Figure 2. The stress-strain curve of shape memory alloy.

Generally, in LSP the thickness of target material is relatively large enough, and thereby the target can be approximately considered as infinitely thick in our study. The eventual shock effects on SMA target, characterized by the plastically affected depth along the central axis of the impact region, L_p , and surface residual stress at the center of the impact region, σ_m , should be a function of the governing parameters characterizing the laser and the metallic target,

$$L_p = f_1(P_m, \tau, R, E_A, E_M, E_{tr}, E_p, \rho, \nu, \sigma_s^{AM}, \sigma_f^{AM}, \sigma_s^{MA}, \sigma_f^{MA}, \sigma_y^M, \gamma, b_A, c_A, b_M, c_M) \quad (1)$$

$$\sigma_m = f_2(P_m, \tau, R, E_A, E_M, E_{tr}, E_p, \rho, \nu, \sigma_s^{AM}, \sigma_f^{AM}, \sigma_s^{MA}, \sigma_f^{MA}, \sigma_y^M, \gamma, b_A, c_A, b_M, c_M) \quad (2)$$

Taking pressure duration τ , martensite elastic modulus E_M and density ρ as a unit system, the following dimensionless relationship can be obtained:

$$\frac{L_p}{R} = f_1\left(\frac{P_m}{\sigma_y^M}, \frac{\tau}{R/\sqrt{E_M/\rho}}, \frac{E_A}{E_M}, \frac{E_{tr}}{E_M}, \frac{E_p}{E_M}, \frac{\sigma_s^{AM}}{E_A}, \frac{\sigma_f^{AM}}{E_M}, \frac{\sigma_s^{MA}}{E_M}, \frac{\sigma_f^{MA}}{E_A}, \frac{\sigma_y^M}{E_M}, \frac{c_A}{\sqrt{E_A/\rho}}, \frac{c_M}{\sqrt{E_M/\rho}}, \gamma, b_A, b_M, \nu\right) \quad (3)$$

$$\frac{\sigma_m}{\sigma_y^M} = f_2\left(\frac{P_m}{\sigma_y^M}, \frac{\tau}{R/\sqrt{E_M/\rho}}, \frac{E_A}{E_M}, \frac{E_{tr}}{E_M}, \frac{E_p}{E_M}, \frac{\sigma_s^{AM}}{E_A}, \frac{\sigma_f^{AM}}{E_M}, \frac{\sigma_s^{MA}}{E_M}, \frac{\sigma_f^{MA}}{E_A}, \frac{\sigma_y^M}{E_M}, \frac{c_A}{\sqrt{E_A/\rho}}, \frac{c_M}{\sqrt{E_M/\rho}}, \gamma, b_A, b_M, \nu\right) \quad (4)$$

There are 16 inherent dimensionless parameters: $\zeta_1 = \frac{P_m}{\sigma_y^M}$, $\zeta_2 = \frac{\tau}{R/\sqrt{E_M/\rho}}$, $\zeta_3 = \frac{E_A}{E_M}$, $\zeta_4 = \frac{E_{tr}}{E_M}$, $\zeta_5 = \frac{E_p}{E_M}$, $\zeta_6 = \frac{\sigma_s^{AM}}{E_A}$, $\zeta_7 = \frac{\sigma_f^{AM}}{E_M}$, $\zeta_8 = \frac{\sigma_s^{MA}}{E_M}$, $\zeta_9 = \frac{\sigma_f^{MA}}{E_A}$, $\zeta_{10} = \frac{\sigma_y^M}{E_M}$, $\zeta_{11} = \frac{c_A}{\sqrt{E_A/\rho}}$, $\zeta_{12} = \frac{c_M}{\sqrt{E_M/\rho}}$, $\zeta_{13} = \gamma$, $\zeta_{14} = b_A$, $\zeta_{15} = b_M$, $\zeta_{16} = \nu$.

The physical meanings of the dimensionless parameters are as follows:

$\frac{P_m}{\sigma_y^M}$: represents the capacity of the plastic deformation.

$\tau/(R/\sqrt{E_M/\rho})$: represents the ratio of loading duration to unloading duration in the target.

$\frac{E_A}{E_M}, \frac{E_{tr}}{E_M}, \frac{E_p}{E_M}$: represent the characteristic austenite elastic modulus, the transformation hardening modulus, and the plastic modulus.

$\frac{\sigma_s^{AM}}{E_A}, \frac{\sigma_f^{AM}}{E_M}, \frac{\sigma_s^{MA}}{E_M}, \frac{\sigma_f^{MA}}{E_A}$: represent the elastic strain of the start of martensite transformation, the finish of martensitic transformation, the start of reverse transformation, and the finish of reverse transformation, respectively.

$\frac{\sigma_y^M}{E_M}$: represents the elastic deformation limit.

$\frac{c_A}{\sqrt{E_A/\rho}}$, $\frac{c_M}{\sqrt{E_M/\rho}}$: represent the characteristic longitudinal sound speed of austenite and martensite, respectively.

γ , b_A , b_M : are adiabatic exponent and constant of Hugoniot equation of state of the target, respectively.

ν : represents the Poisson's ratio of target.

If the target material is fixed, the 14 material related dimensionless parameters in the bracket on the right hand side in Equations (3) and (4) remain constant. Consequently, simpler relations can be obtained,

$$\frac{L_p}{R} = f_1\left(\frac{P_m}{\sigma_y^M}, \frac{\tau}{R/\sqrt{E_M/\rho}}\right) \quad (5)$$

$$\frac{\sigma_m}{\sigma_y^M} = f_2\left(\frac{P_m}{\sigma_y^M}, \frac{\tau}{R/\sqrt{E_M/\rho}}\right) \quad (6)$$

It indicates that a scaling law holds for laser shock peening effects of shape memory alloys. From Equations (5) and (6), the same distribution of residual stress will be induced in the target, while the dimensionless parameters P_m/σ_y^M and $\tau/(R/\sqrt{E_M/\rho})$ are unchanged in LSP process.

3. Numerical Simulation of LSP process of SMAs

3.1. Constitutive Model of Shape Memory Alloys

The superelastic behavior of shape memory alloys is observed during loading and unloading at the temperature above the finish temperature of austenite transformation and is associated with the deformation induced martensite transformation and the reverse transformation upon unloading. The constitutive model considers simultaneously the phase transformation and plasticity of deformation induced martensite, which is different from plastic models of traditional metals.

Based on the assumption of small deformation, total strain consists of three parts: the first part, ε^e , is the elastic strain; the second part, ε^{tr} , is the transformation strain from austenite to deformation induced martensite phase; the third part ε_M^p is the plastic strain induced by the irreversible plastic slip of martensite under high stress,

$$\varepsilon = \varepsilon^e + \varepsilon^{tr} + \varepsilon_M^p \quad (7)$$

By setting the internal variable as the martensite volume fraction z , the elastic stress-strain relationship is

$$\sigma = \mathbf{D}(z) : [\varepsilon - \varepsilon^{tr} - \varepsilon_M^p] \quad (8)$$

The variations of elastic modulus matrix $\mathbf{D}(z)$ during the deformation induced martensite transformation can be described by setting the dependence of \mathbf{D} on the internal variable z ,

$$\mathbf{D}(z) = (1 - z)\mathbf{D}_A + z\mathbf{D}_M \quad (9)$$

\mathbf{D}_A and \mathbf{D}_M are equivalent elastic modulus tensors of austenite and martensite phase, respectively.

3.1.1. Transformation Model

Martensitic transformation is important for shape memory alloys because it is the cause of shape memory effect and superelasticity. The generalized plasticity model is firstly employed by Lubliner and Auricchio [14] to describe martensitic transformation and reverse transformation of shape memory alloys. A Drucker–Prager-type transformation surface is introduced:

$$F_y^{MA} = \bar{\sigma} - \sigma_s^{MA}(z) = 0, \text{ forward transformation} \quad (10a)$$

$$F_y^{AM} = \bar{\sigma} - \sigma_s^{AM}(z) = 0, \text{ reverse transformation} \quad (10b)$$

where, $\bar{\sigma}$ is the equivalent stress, z is the volume fraction of martensite, and $\sigma_s^{MA}(z)$ and $\sigma_s^{AM}(z)$ are the start stresses of forward transformation and reverse transformation respectively.

Similar to the classical plasticity, the increment of transformation strain obeys the normality rule. The increment of transformation strain is normal to the transformation surface in the stress space as,

$$d\varepsilon^{tr} = d\gamma \frac{\partial F_y^{AM}(\sigma, z)}{\partial \sigma}, d\gamma > 0, \text{ forward transformation} \quad (11a)$$

$$d\varepsilon^{tr} = d\gamma \frac{\partial F_y^{MA}(\sigma, z)}{\partial \sigma}, d\gamma < 0, \text{ reverse transformation} \quad (11b)$$

where $d\gamma$ is the increment of multiplier of transformation strain. The hardening behavior of transformation can be described by transformation hardening modulus E_{tr} .

3.1.2. Plasticity Model

After the martensitic transformation, plastic deformation occurs in the deformation induced martensite if the applied load is higher than the yield stress of the martensite. Assuming that the plastic deformation obeys the Von Mises yielding condition,

$$F_y^{MP}(\sigma, \varepsilon_p) = \bar{\sigma} - \sigma_y^M(\varepsilon_p) = 0 \quad (12)$$

where, $\bar{\sigma}$ is equivalent stress and σ_y^M represents the yielding stress of deformation induced martensite.

The increment of plastic strain is given by

$$d\varepsilon_p = d\lambda \frac{\partial F_y^{MP}(\sigma, \varepsilon_p)}{\partial \sigma} \quad (13)$$

where, $d\lambda$ is the increment of multiplier of plastic strain. The plastic hardening behavior of martensite can be described by plastic hardening modulus E_p .

3.2. Finite Element Modeling

As the LSP process involves high-speed impact and dynamic wave propagation, explicit time integration finite element codes need to be employed. In this respect, the ABAQUS/Explicit code is used to simulate the LSP process. The full development of plastic deformation in the material during the LSP process takes much longer than the duration of the pulse pressure so the calculation time should be sufficiently long.

3.2.1. Finite Element Model

As shown in Figure 3, a two-dimensional axisymmetric finite element model is developed to simulate the LSP process of SMA material, in which the dimensionless coordinates $r^* = \frac{r}{R}$, and $y^* = \frac{y}{R}$ are used. LSP is a highly localized process. The size of the laser-treated region is very small compared to the size of the target material. Finer elements are used to model the laser treated region and coarse elements represent the rest of the component. The dimension of the finer meshed region depends on the size of the laser spot. Researchers have chosen 2 times or 3.5 times the laser spot size for the finer meshed region [15–17]. In this work, three times the laser spot size is used. The size of the coarse meshed region is chosen as eight times the laser spot size. CAX4R (continuum axisymmetric 4 noded reduced integration) elements are used in the model. In order to simulate the peening effect of shock wave passing the target material only once, it is necessary to avoid the shock wave reflecting back into the target material, i.e., setting up a non-reflective boundary condition. Firstly, a thin layer of material with large damping property is bonded to the lower boundary of the target to dissipate the energy of shock wave. Then a thin flyer is attached to the back free surface of the energy dissipation layer by using a surface to surface contact. The thickness of the flyer is larger than 2 times the propagation distance of shock wave during the pressure duration.

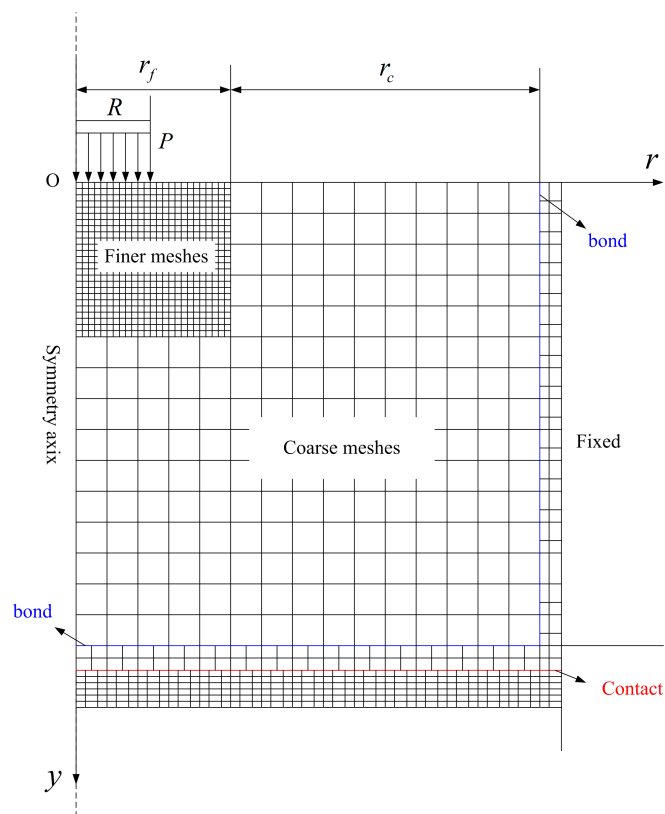


Figure 3. 2D axisymmetric finite element simulation model.

The SMA target is shocked by the dimensionless pressure $p(t)/\sigma_y^M$ with uniform distribution throughout the laser treated region. In a typical LSP process, the peak pressure of laser induced shock is at the level of several GPa, and the shock duration is in the nanosecond scale. Although the pressure-time history is usually described as a Gaussian temporal profile, it is very close to a triangular ramp because of the very narrow pulse duration, as shown in Figure 4. Therefore, in this work, the pressure is assumed to have a triangular profile. The pressure rises linearly to the peak pressure, P_m , and then declines linearly in the period of $2t_d$ [9,18].

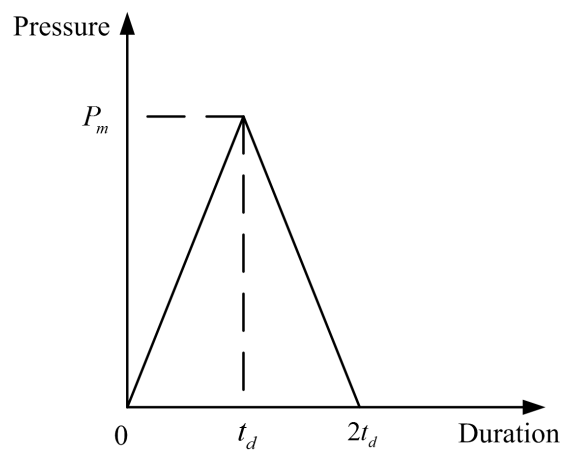


Figure 4. Pressure-time history of laser shock peening (LSP).

In the simulation, a user-material subroutine (VUMAT) for shape memory alloy based on the generalized plasticity of Lubliner and Auricchio [14] was incorporated into the finite element analysis. The material properties of shape memory alloy are given in Table 1. The constitutive parameters as shown in Figure 2 are obtained from the quasi-static tensile stress-strain curve of a NiTi alloy used in the following LSP experiments. The Mie-Grüneisen EOS coefficients are taken from reference [19]. The corresponding dimensionless parameters are kept constant in the numerical simulation and listed in Table 2.

Table 1. Mechanical parameters of NiTi shape memory alloys.

Material Properties, Units	Value
Young's modulus of austenite, E_A (GPa)	80
Young's modulus of martensite, E_M (GPa)	40
Poisson's ratio, ν	0.33
Density, ρ (g/cm ³)	6.45
Start stress of transformation, σ_s^{AM} (MPa)	500
Finish stress of transformation, σ_f^M (MPa)	550
Start stress of reverse transformation, σ_s^{MA} (MPa)	300
Finish stress of reverse transformation, σ_f^{MA} (MPa)	250
Transformation modulus, E_{tr} (GPa)	2.86
Yield stress of martensite, σ_y^M (MPa)	1100
Plastic modulus, E_p (GPa)	4.0
Sound velocity of austenite, c_A (m/s)	5.12×10^3
Sound velocity of matensite, c_M (m/s)	3.56×10^3
Mie-Grüneisen constant of austenite, b_A	-3.88
Mie-Grüneisen constant of austenite, b_M	4.87
Adiabatic exponent, γ	2.0

Table 2. Material related dimensionless parameters.

$\frac{E_A}{E_M}$	$\frac{E_{tr}}{E_M}$	$\frac{E_p}{E_M}$	$\frac{\sigma_s^{AM}}{E_A}$	$\frac{\sigma_f^{AM}}{E_M}$	$\frac{\sigma_s^{MA}}{E_M}$	$\frac{\sigma_f^{MA}}{E_A}$
2.00	0.071	0.1	6.25×10^{-3}	1.38×10^{-2}	7.50×10^{-3}	3.12×10^{-3}
$\frac{\sigma_y^M}{E_M}$	$\frac{c_A}{\sqrt{E_A/\rho}}$	$\frac{c_M}{\sqrt{E_M/\rho}}$	γ	b_A	b_M	ν
2.75×10^{-2}	1.45	1.43	2.00	-3.88	4.87	0.33

3.2.2. Convergence Validation of Numerical Models

The convergence of the numerical simulation results was validated by comparing with the experimental results for traditional steel material from Ballard et al. [11]. The simulated surface residual stresses are shown in Figure 5, where the minimum length of elements $\zeta^* = L_{min}/R = 0.006$, the time increment $\Delta t^* = \Delta t/\tau = 0.005$, and the total time $t^* = t/\tau = 5000$. The simulated result agrees well with the experimental result, which validates the convergence of the numerical simulations for $\zeta^* = 0.006$, $\Delta t^* = 0.005$, and $t^* = 5000$. Therefore, the same values of the ζ^* , Δt^* , and t^* are taken in the simulation of LSP process of SMA materials.

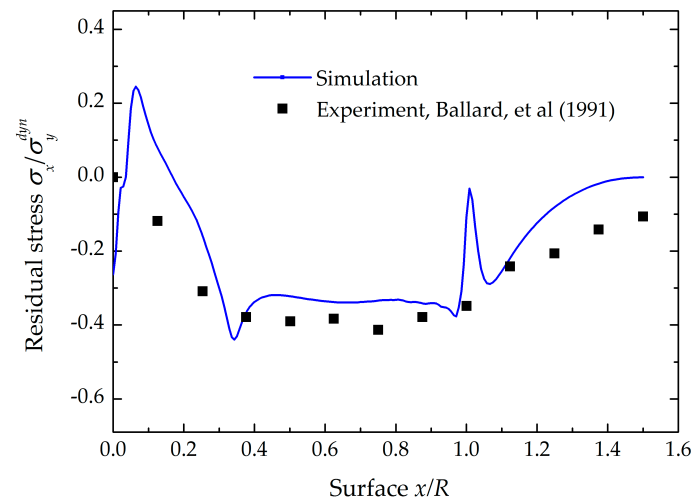


Figure 5. Residual stresses along x/R of the present simulated results and the experimental measurement of Ballard et al. (1991), in which the same pressure and material are used in the simulation. The minimum length of elements $\xi^* = 0.006$, the time increment $\Delta t^* = 0.005$ and the total time $t^* = 5000$ are used in the simulation.

3.2.3. Scheme of Numerical Simulation for LSP

To validate the scaling law derived in Section 2, a parameter study is conducted to investigate the influence of dimensionless parameters on shock effects. Two groups of simulations are conducted and the parameters are shown as the following:

1. Shock effects for constant dimensionless peak pressure and laser duration are simulated, in which the dimensionless peak pressure P_m/σ_y^M is set as 4.55, and the dimensionless laser duration $\tau/(R/\sqrt{E_M/\rho})$ is set as 0.025. For the constant dimensionless laser duration $\tau/(R/\sqrt{E_M/\rho})$, the sets of the parameters (R and τ) are (0.5 mm, 5.0 ns), (1.0 mm, 10.0 ns), (1.5 mm, 15.0 ns), and (2.0 mm, 20.0 ns).
2. Parameter study: $P_m/\sigma_y^M \in (2.73, 10.91)$, $\tau/(R/\sqrt{E_M/\rho}) \in (0.0025, 0.1000)$, analyzing the influence of the dimensionless parameters $\tau/(R/\sqrt{E_M/\rho})$ and P_m/σ_y^M .

4. Numerical Results

Simulation results for simulation group 1 are shown in Figure 6. As the axisymmetry model is used, the residual stress in impact region is calculated as $\sigma_{res} = \sqrt{\sigma_{rr}^2 + \sigma_{\theta\theta}^2}$. We define the depth of the plastically affected region as the distance from the point, where residual stress changes sign from compressive to tensile, to the laser treated surface. From Figure 6, it can be seen that the dimensionless surface residual stress, and the plastically affected depth for the four sets of parameters are all about 0.715 and 0.198 respectively. The distribution of surface residual stress, and residual stress distribution in depth of the four sets of parameters are almost the same, which demonstrates that the scaling law of LSP processing of shape memory alloys holds. The scaling law is useful in LSP experiments, because the number of the independent parameters can be reduced and the experimental efficiency can be improved significantly to obtain an optimized parameter window.

As shown in Figure 6b, the residual stress in the shape memory alloys shows a plateau of compressive stress, which is different from the traditional metallic material where the residual stress gradually changes from the maximum compressive stress near the surface to nearly zero along the depth. Shape memory alloys can experience martensitic transformation in loading and reverse transformation upon unloading. The appearance of the plateau in the residual stress along the depth is due to the residual martensitic transformation. The plateau corresponds to the transaction

region from martensite to austenite. The magnitude of dimensional residual stress in the plateau region is about -0.333 , and the component along radius and circular is -0.233 , which is close to dimensionless start stress of the reverse transformation, -0.227 . It is possible to introduce a relatively uniform residual stress beneath the surface of shape memory alloys by changing the start stress of the reverse transformation.

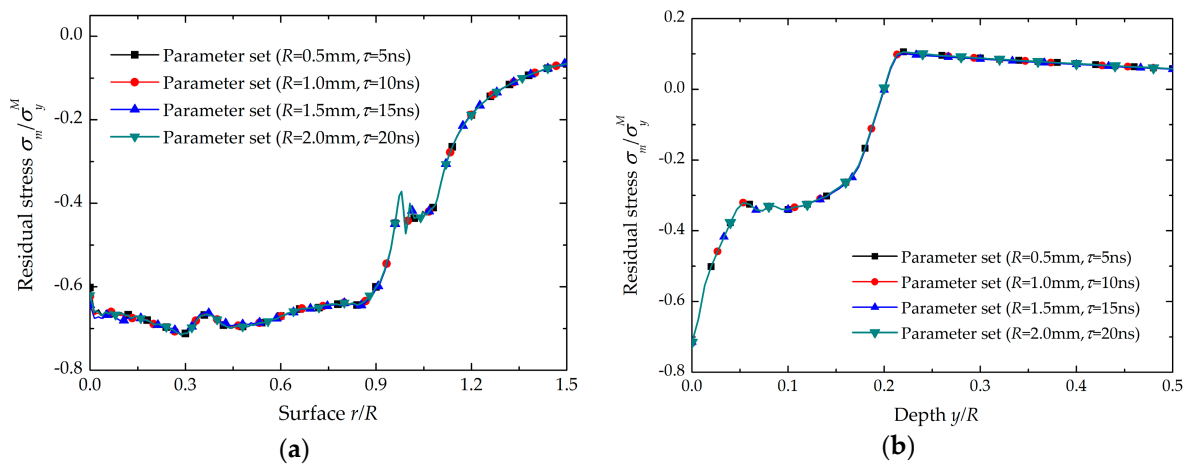


Figure 6. Results of simulation group 1: (a) Surface residual stress distribution along the radius; (b) Residual stress distribution in depth at the center of the shock region for sets of parameters (R and τ) are (0.5 mm, 5.0 ns), (1.0 mm, 10.0 ns), (1.5 mm, 15.0 ns), and (2.0 mm, 20.0 ns). The dimensionless peak pressure is fixed as 4.55. The other dimensionless parameters are kept constant as given in Table 2.

Simulation group 2 simulates the influence of laser duration and peak pressure on shock effects. Simulation results are shown in Figure 7. Figure 7a shows the influence of laser duration and peak pressure on the maximum residual stress. It can be seen that the maximum residual stress is almost independent with pressure duration when peak pressure is less than 5.45. When the peak pressure is over 5.45, the maximum has the trend to decrease with increasing the pressure duration. This is because a round spot is used in our simulation. Hu et al. [20] found that “residual stress hole” effect is remarkable when target is treated by a round laser spot, which is attributed to radial rarefaction waves coming from edges of the impact after the interaction and focalizing simultaneously to its center.

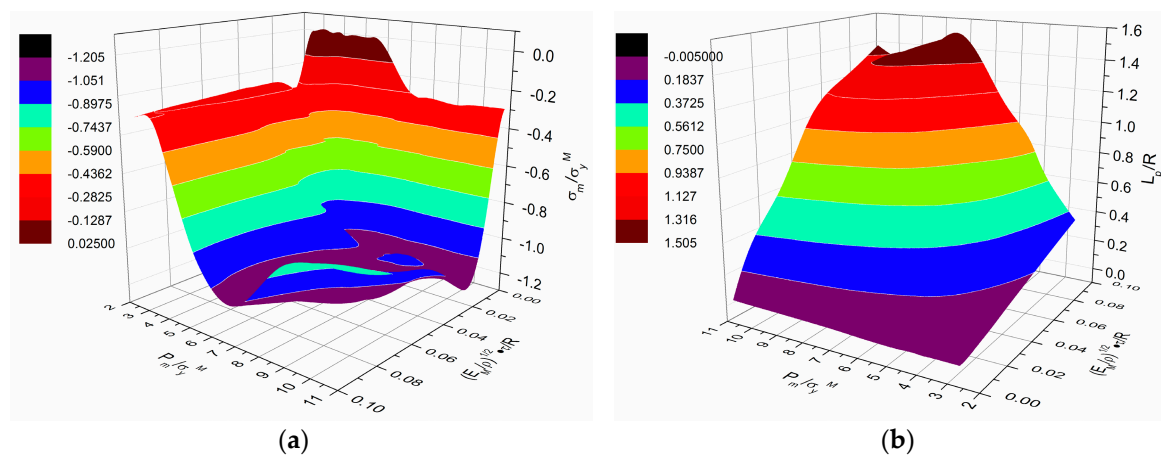


Figure 7. Results of simulation group 2: (a) Influence of laser duration and peak pressure on maximum residual stress; (b) Influence of laser duration and peak pressure on plastically affected depth. The dimensionless peak pressure ranges from 2.73 to 10.91, the dimensionless laser duration ranges from 0.0025 to 0.1. The other dimensionless parameters are kept constant as given in Table 2.

Figure 7b shows the influence of laser duration and peak pressure on plastically affected depth. The plastically affected depth increases monotonically with increasing the pressure duration when the peak pressure is less than 7.27. When the peak pressure exceeds 7.27, the plastically affected depth exhibits nonlinear characteristics with increasing pressure duration. The plastically affected depth increases clearly with the peak pressure when the pressure duration is less than 0.0747. However when the pressure duration exceeds 0.0747, the plastically affected depth increases at the beginning and then slightly decreases with increasing the peak pressure.

Figure 8a shows the relationship between the plastically affected depth and the laser duration at different peak pressure. When the peak pressure is less than 7.27, the plastically affected depth increases linearly with increasing the pressure duration for different peak pressure, which is consistent with traditional metals. Ballard et al. [11], and Peyre et al. [21] found the plastically affected depth is linear with the pressure duration for steel and aluminum alloy by theoretical analysis. When the peak pressure is over 7.27, the plastically affected depth exhibits nonlinear characteristics with increasing the pressure duration. Thus when the peak pressure is less than 7.27, the Equation (5) can be expressed as follows,

$$\frac{L_p}{R} = g\left(\frac{P_m}{\sigma_y^M}\right) * \frac{\tau}{R/\sqrt{E_M/\rho}} \quad (14)$$

It can be seen that the plastically affected depth is independent of laser spot size R . In order to obtain the function of peak pressure, Equation (14) can be expressed as follows,

$$\frac{L_p}{\sqrt{E_M/\rho} * \tau} = g\left(\frac{P_m}{\sigma_y^M}\right) \quad (15)$$

Figure 8b shows the relationship between the dimensionless plastically affected depth $L_p/(\sqrt{E_M/\rho} * \tau)$ and the dimensionless peak pressure P_m/σ_y^M at different dimensionless pressure duration. The dimensionless plastically affected depth $L_p/(\sqrt{E_M/\rho} * \tau)$ increases almost linearly with increasing the dimensionless peak pressure when the peak pressure is less than 7.27. Thus the function of peak pressure can be obtained by linearly fitting when the peak pressure is less than 7.27. The dimensionless plastically affected depth $L_p/(\sqrt{E_M/\rho} * \tau)$ could be fitted by linear functions with high correlations of $R^2 = 0.9815$,

$$\frac{L_p}{\sqrt{E_M/\rho} * \tau} = 2.625 * \left(\frac{P_m}{\sigma_y^M} - 1.682\right) \quad (16)$$

Therefore, the plastically affected depth increases linearly with the pressure duration and the peak pressure. The function is similar with Ballard et al.'s for traditional metals [11]. According to one dimensional strain theory [22], plastic deformation occurs only when the pressure is above the Hugoniot elastic limit (HEL). From Equation (16), the relationship between HEL and the yield stress for shape memory alloys can be expressed as,

$$\text{HEL} = 1.682\sigma_y^M \quad (17)$$

where σ_y^M is the yield strength of deformation induced martensite.

For traditional metals, HEL is related to dynamic yield strength according to [23]:

$$\text{HEL} = \frac{1 - \nu}{1 - 2\nu} \sigma_y^{dyn} \quad (18)$$

where ν is the Poisson's ratio and σ_y^{dyn} is the dynamic yield strength at high strain rates. When ν is 0.33, Equation (18) can be expressed as $\text{HEL} = 1.970\sigma_y^{dyn}$. Compared with Equation (17), it can be seen that the coefficient is different from shape memory alloys. This is attributed to the martensitic transformation before plasticity when shape memory is treated with laser induced shock. For shape

memory alloy, HEL cannot be obtained from Equation (18) because the martensitic transformation is inelastic.

However, when the peak pressure is exceeds 7.27, the dimensionless plastically affected depth $L_p/(\sqrt{E_M/\rho} * \tau)$ increases slightly or even decreases with increasing the dimensionless peak pressure. This is probably due to surface wave release wave focusing and amplifying from the edges of the impacts thus modifying the residual stress field [21]. The target will be compressed when the shock wave propagates. According to theory of surface waves [22], the particles of the surface will be dilatated laterally because of the Poisson effect. Thus a dilatation wave will be initiated when a compressive wave arrives. The dilatation wave will decrease the surface residual stress and plastically affected depth. The magnitude of dilatation wave is related with pressure duration and peak pressure. When pressure duration and peak pressure are small, the magnitude of surface wave is small and has little influence on the maximum residual stress and the plastically affected depth. But when pressure duration and peak pressure exceed some values, the magnitude of surface wave becomes larger, and has clear influence on the maximum residual stress and the plastically affected depth. The maximum residual stress and plastically affected depth will decrease when increasing the peak pressure and pressure duration when pressure duration and peak pressure exceed some values, as shown in Figure 8.

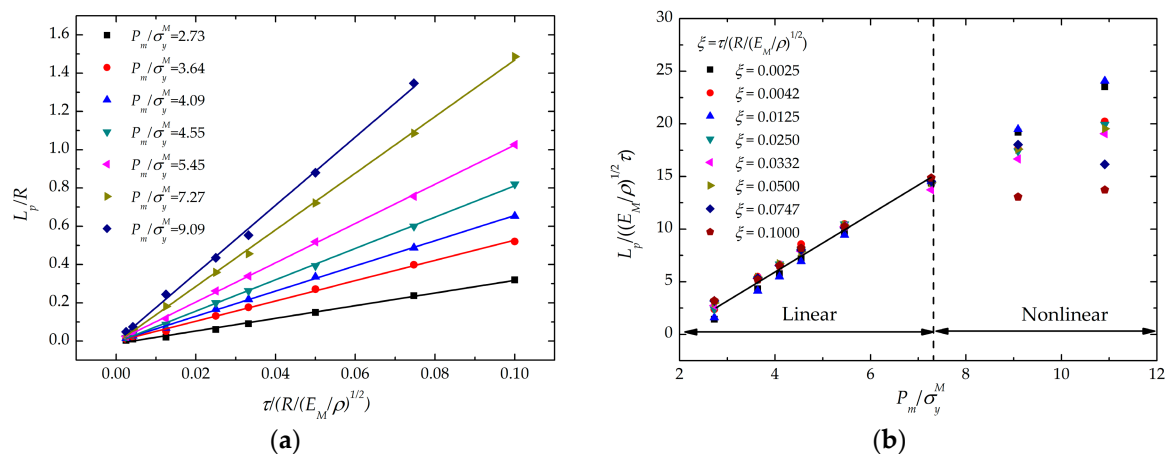


Figure 8. (a) Influence of pressure duration on the plastically affected depth at different peak pressure; (b) Influence of peak pressure on the plastically affected depth at different pressure duration. The material related dimensionless parameters are kept constant as given in Table 2.

5. Experimental Validation

5.1. Experimentals

Polycrystalline NiTi sheets were purchased from GEE Shape Memory Alloy Inc. (Beijing, China). The nominal alloy composition was Ni-50.9% and Ti-49.1% (at %). The transformation temperatures determined by differential scanning calorimeter (DSC, Perkin Elmer Diamond) were $M_s = 285$ K, $M_f = 274$ K, $A_s = 277$ K, $A_f = 286$ K respectively. Therefore, the alloy is in austenite phase and exhibits superelasticity behavior under stress at room temperature. The specimen (10.0 mm \times 10.0 mm \times 1.0 mm) was cut from the sheet using wire-electrode cutting machine. Before LSP, the specimen surface was ground using a sequence of increasing grit sandpaper followed by final polishing with 0.05 μ m SiO₂ paste.

The LSP experiment was performed with a Q-switched high power Nd:YAG pulse laser operating at 1064 nm wavelength. The output energy of laser beam is 2.4 J per shot. The temporal profile of the laser pulse is in the near Gaussian shape and the full width at half maximum (FWHM) is approximately 10 ns. The spatial profile of the laser pulse is approximately uniform. The diameter of the focused

laser beam on the specimen varies from 2.8 to 3.2 mm, resulting in the laser power density achieved at the specimen surface varying from 2.8 to 4.4 GW/cm² in this study. An Al foil (0.05 mm thick) or a self-adhesive black paint (0.18 mm thick) was then attached to the target surface as absorption layer, confined by a BK-7 glass or water on top against the laser irradiation. The combination of different confined overlay and absorbed layer was used to obtain various shock pressures. One group of specimen used water as confined overlay and black paint as absorbed layer to obtain lower shock pressure while the other group used BK-7 glass as confined overlay and Al foil as absorbed layer to obtain higher shock pressure.

After the laser shock process, the Vickers hardness of the peened sample was measured by a micro-hardness tester MH-5L. The plastically affected depth in NiTi sample was characterized with micro-hardness measurements on the cross-section of peened sample. A diamond Vickers indenter with a face angle of 136° was used. The hardness was measured under a load of 200 g and a holding time of 10 s at room temperature. Indentations were conducted with a special interval of at least 250 µm to avoid interference.

5.2. Experimental Results

The experimental conditions and corresponding results of induced peak pressure and plastically affected depth are summarized in Table 3. The peak pressure induced by laser pulse can be estimated by Fabbro's model [24],

$$P_m(\text{GPa}) = 0.01 \sqrt{\frac{\alpha}{2\alpha + 3}} \sqrt{Z(\text{g} \cdot \text{cm}^{-2} \cdot \text{s}^{-1})} \sqrt{I_0(\text{GW} \cdot \text{cm}^{-2})} \quad (19)$$

where α is the fraction of the internal energy devoted to the thermal energy (typically, $\alpha \approx 0.25$), I_0 is the laser power density and $Z = 2Z_1Z_2/(Z_1 + Z_2)$ is the reduced shock impedance between the absorption material (black paint, shock impedance $1.98 \times 10^5 \text{ g} \cdot \text{cm}^{-2} \cdot \text{s}^{-1}$; Al, shock impedance $1.47 \times 10^6 \text{ g} \cdot \text{cm}^{-2} \cdot \text{s}^{-1}$) and the confining medium (water, shock impedance $1.45 \times 10^5 \text{ g} \cdot \text{cm}^{-2} \cdot \text{s}^{-1}$; BK-7 glass, shock impedance $1.44 \times 10^6 \text{ g} \cdot \text{cm}^{-2} \cdot \text{s}^{-1}$). The pressure transmitted into the NiTi material is enhanced due to the impedance mismatch between the absorption material and target material (NiTi, shock impedance $3.44 \times 10^6 \text{ g} \cdot \text{cm}^{-2} \cdot \text{s}^{-1}$) [25]. As shown in Table 3, the peak shock pressure varies from 3.8 to 8.8 GPa for the combination of different confined overlay and absorbed layer.

The hardness-depth profiles on the cross-section of peened specimen are shown in Figure 9. Due to the peening effect, the hardness increases in the surface layer and then decreases to the value of untreated specimen at a certain depth. This depth is taken as the plastically affected depth. As shown in Figure 9a, the plastically affected depth is about 200–300 µm for the specimen peened using water as confined overlay and black paint as absorbed layer, while this depth can reach 500–600 µm for specimen peened using BK-7 glass as confined overlay and Al foil as absorbed layer.

Table 3. Experimental results under the condition of different confined overlay and absorbed layer.

Laser Power Density (GW/cm ²)	Confined Overlay	Absorbed Layer	Laser Spot Diameter (mm)	Peak Pressure (GPa)	Plastically Affected Depth (mm)
3.4	water	black paint	2.96	3.8	0.25 ± 0.10
3.8	water	black paint	2.78	4.0	0.25 ± 0.05
4.4	water	black paint	2.60	4.3	0.30 ± 0.10
2.8	BK-7 glass	Al foil	3.26	7.5	0.50 ± 0.05
3.4	BK-7 glass	Al foil	2.96	8.3	0.60 ± 0.10
3.8	BK-7 glass	Al foil	2.78	8.8	0.60 ± 0.05

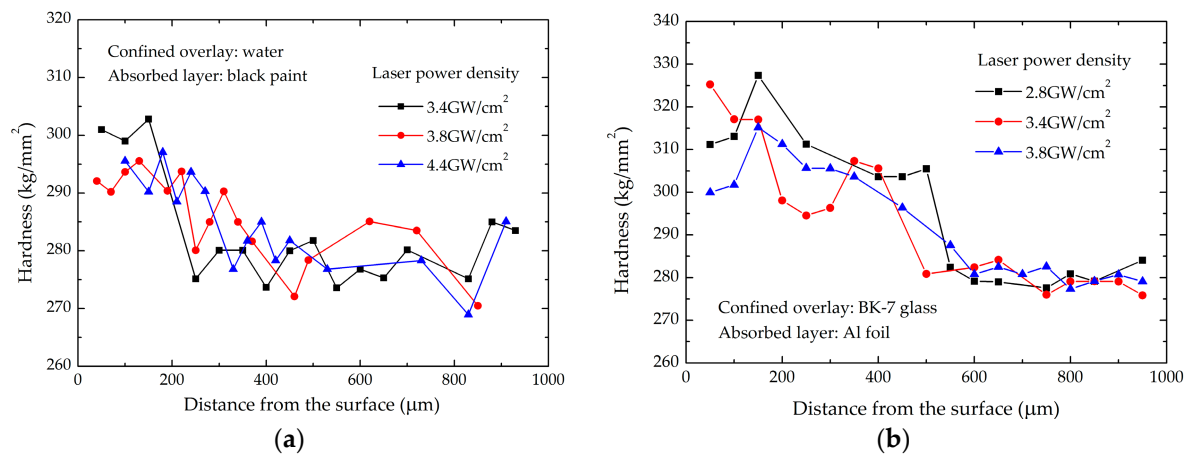


Figure 9. Hardness-depth profile of laser-shock-peened NiTi specimen: (a) water as confined overlay and black paint as absorbed layer; (b) BK-7 glass as confined overlay and Al foil as absorbed layer.

The experimental results of plastically affected depth are compared with the derived scaling law in Figure 10 according to Equation (16), where martensite elastic modulus E_M , density ρ and the yield stress of deformation induced martensite σ_y^M are from Table 1 and the pressure duration τ is 20 ns. It can be seen that the linear relation in the terms of the dimensionless variables as shown in Equation (16) matches fairly well with the experiment results. Due to the limit of experimental conditions, we could not conduct the LSP experiment at much higher peak pressure. Therefore, the validation of nonlinear characteristic of scaling law needs further investigation.

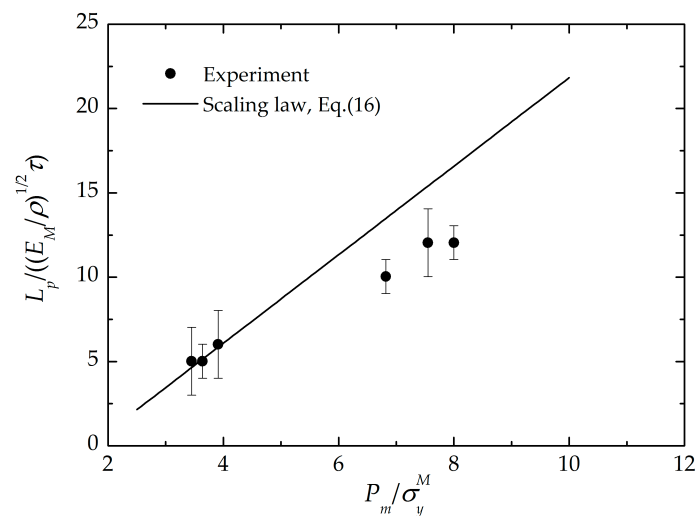


Figure 10. Comparison of experimental results of plastically affected depth with scaling law.

6. Conclusions

Scaling law in laser shock processing of shape memory alloys has been investigated. The main conclusions are as follows:

1. The essential dimensionless parameters controlling the residual stress distribution and plastically affected depth were found to be dimensionless pressure duration and peak pressure.
2. The residual stress and the plastically affected depth both show the two-stage characteristic depending on the peak pressure. The maximum residual stress is almost independent with pressure duration and increases sharply with increasing peak pressure when peak pressure is

less than 5.45. However, when peak pressure exceeds 5.45, the maximum residual stress has the trend to decrease with increasing the pressure duration, and increases slowly or even decreases with increasing peak pressure. The plastically affected depth increases linearly with increasing the pressure duration and peak pressure when the peak pressure is less than 7.27. When the peak pressure is exceeds 7.27, the plastically affected depth shows nonlinear characteristics. This two-stage characteristic is due to surface release waves focusing and amplifying from edges of the impact.

3. The scaling relation of plastically affected depth with peak pressure is validated with experimentally measured hardness-depth profile of a laser-shock-peened NiTi specimen.

Acknowledgments: The authors would like to thank the National Natural Science Foundation of China (Grant No. 11002150, 11332011, 11402277) and the Basic Research Equipment Project of Chinese Academy of Sciences (YZ200930) for financial support.

Author Contributions: Xi Wang and Chenguang Huang conceived and design the analysis, simulation and experiment; Weiguang Xia performed the dimensional analysis; Weiguang Xia and Xianqian Wu performed the simulation and experiments; Xi Wang wrote the paper.

Conflicts of Interest: The authors declare no conflict of interest.

References

1. Kazuhiro, O.; Clarence Marvin, W. *Shape Memory Materials*; Cambridge University Press: Cambridge, UK, 1999; ISBN 0521663849.
2. Grant, D.M.; Green, S.M.; Wood, J.V. The surface performance of shot peened and ion implanted NiTi shape memory alloy. *Acta Metall. Mater.* **1995**, *43*, 1045–1051. [[CrossRef](#)]
3. Koike, J.; Parkin, D.M.; Nastasi, M. Crystal-to-amorphous transformation of NiTi induced by cold-rolling. *J. Mater. Res.* **1990**, *5*, 1414–1418. [[CrossRef](#)]
4. Sergueeva, A.V.; Song, C.; Valiev, R.Z.; Mukherjee, A.K. Structure and properties of amorphous and nanocrystalline NiTi prepared by severe plastic deformation and annealing. *Mater. Sci. Eng. A* **2003**, *339*, 159–165. [[CrossRef](#)]
5. Karaman, I.; Karaca, H.; Luo, Z.; Maier, H.J. The effect of severe marforming on shape memory characteristics of a Ti-rich NiTi alloy processed using equal channel angular extrusion. *Metall. Mater. Trans. A* **2003**, *34*, 2527–2539. [[CrossRef](#)]
6. Liao, Y.; Ye, C.; Lin, D.; Suslov, S.; Cheng, G. Deformation induced martensite in NiTi and its shape memory effects generated by low temperature laser shock peening. *J. Appl. Phys.* **2012**, *112*, 033515. [[CrossRef](#)]
7. Ye, C.; Suslov, S.; Fei, X.; Cheng, G.J. Bimodal nanocrystallization of NiTi shape memory alloy by laser shock peening and post-deformation annealing. *Acta Mater.* **2011**, *59*, 7219–7227. [[CrossRef](#)]
8. Montross, C.S.; Wei, T.; Ye, L.; Clark, G.; Mai, Y.-W. Laser shock processing and its effects on microstructure and properties of metal alloys: A review. *Int. J. Fatigue* **2002**, *24*, 1021–1036. [[CrossRef](#)]
9. Ding, K.; Ye, L. *Laser Shock Peening: Performance and Process Simulation*; CRC Press: Boca Raton, FL, USA, 2006; ISBN 0849334446.
10. Luo, K.Y.; Lu, J.Z.; Zhang, Y.K.; Zhou, J.Z.; Zhang, L.F.; Dai, F.Z.; Zhang, L.; Zhong, J.W.; Cui, C.Y. Effects of laser shock processing on mechanical properties and micro-structure of ANSI 304 austenitic stainless steel. *Mater. Sci. Eng. A* **2011**, *528*, 4783–4788. [[CrossRef](#)]
11. Ballard, P.; Fournier, J.; Fabbro, R. Residual stresses induced by laser-shocks. *J. Phys. IV* **1991**, *1*, 487–494. [[CrossRef](#)]
12. Wu, B.X.; Shin, Y.C. From incident laser pulse to residual stress: A complete and self-closed model for laser shock peening. *J. Manuf. Sci. Eng.-Trans. ASME* **2007**, *129*, 117–125. [[CrossRef](#)]
13. Wu, X.Q.; Tan, Q.M.; Huang, C.G. Geometrical Scaling Law for Laser Shock Peening. *J. Appl. Phys.* **2013**, *114*, 043105. [[CrossRef](#)]
14. Lubliner, J.; Auricchio, F. Generalized plasticity and shape-memory alloys. *Int. J. Solids Struct.* **1996**, *33*, 991–1003. [[CrossRef](#)]
15. Braisted, W.; Brockman, R. Finite element simulation of laser shock peening. *Int. J. Fatigue* **1999**, *21*, 719–724. [[CrossRef](#)]

16. Arif, A.F.M. Numerical prediction of plastic deformation and residual stresses induced by laser shock processing. *J. Mater. Process. Technol.* **2003**, *136*, 120–138. [[CrossRef](#)]
17. Ding, K. Three-dimensional dynamic finite element analysis of multiple laser shock peening processes. *Surf. Eng.* **2003**, *19*, 351–358. [[CrossRef](#)]
18. Ding, K.; Ye, L. Simulation of multiple laser shock peening of a 35CD4 steel alloy. *J. Mater. Process. Technol.* **2006**, *178*, 162–169. [[CrossRef](#)]
19. Meziere, Y.J.E.; Millett, J.C.F.; Bourne, N.K. Equation of state and mechanical response of NiTi during one-dimensional shock loading. *J. Appl. Phys.* **2006**, *100*, 033513. [[CrossRef](#)]
20. Hu, Y.X.; Yao, Z.Q.; Wang, F.; Hu, J. Study on residual stress of laser shock processing based on numerical simulation and orthogonal experimental design. *Surf. Eng.* **2007**, *23*, 470–478. [[CrossRef](#)]
21. Peyre, P.; Fabbro, R.; Merrien, P.; Lieurade, H.P. Laser shock processing of aluminium alloys. Application to high cycle fatigue behaviour. *Mater. Sci. Eng. A* **1996**, *210*, 102–113. [[CrossRef](#)]
22. Wang, L.L. *Foundation of Stress Waves*; Elsevier: Oxford, UK, 2007; ISBN 9780080444949.
23. Johnson, J.N.; Rohde, R.W. Dynamic deformation twinning in shock-loaded iron. *J. Appl. Phys.* **1971**, *42*, 4171–4182. [[CrossRef](#)]
24. Berthe, L.; Fabbro, R.; Peyre, P.; Tollier, L.; Bartnicki, E. Shock waves from a water-confined laser-generated plasma. *J. Appl. Phys.* **1997**, *82*, 2826–2832. [[CrossRef](#)]
25. Millett, J.C.F.; Bourne, N.K. The shock-induced mechanical response of the shape memory alloy, NiTi. *Mater. Sci. Eng. A* **2004**, *378*, 138–142. [[CrossRef](#)]



© 2018 by the authors. Licensee MDPI, Basel, Switzerland. This article is an open access article distributed under the terms and conditions of the Creative Commons Attribution (CC BY) license (<http://creativecommons.org/licenses/by/4.0/>).